# A preliminary study about high-pressure homogenization as a viable alternative to produce powder feedstock for selective laser sintering of biopolymers

Materials Research Proceedings 57 (2025) 154-163 https://doi.org/10.21741/9781644903735-18

# A preliminary study about high-pressure homogenization as a viable alternative to produce powder feedstock for selective laser sintering of biopolymers

Alberto GIUBILINI[1,2,a *], Giovanna COLUCCI[3,b], Manuela GALATI[1,2,c], Giovanni MARCHIANDI[1,2,d], Massimo MESSORI[3,e], Luca IULIANO[1,2,f] and Paolo MINETOLA[1,2,g]

[1]Department of Management and Production Engineering (DIGEP), Politecnico di Torino, Corso Duca degli Abruzzi 24, 10129 Torino, Italy

[2]Integrated Additive Manufacturing Centre (IAM@PoliTO), Politecnico di Torino, Corso Duca degli Abruzzi 24, 10129 Torino, Italy

[3]Department of Applied Science and Technology (DISAT), Politecnico di Torino, Corso Duca degli Abruzzi 24, 10129 Torino, Italy

[a]alberto.giubilini@polito.it, [b]giovanna.colucci@polito.it, [c]manuela.galati@polito.it, [d]giovanni.marchinadi@polito.it, [e]massimo.messori@polito.it, [f]luca.iuliano@polito.it, [g]paolo.minetola@polito.it

**Keywords:** Powder Bed Fusion, Polymers, Sustainable Development

**Abstract.** Selective laser sintering is an established technique for producing complex plastic components, yet its broader adoption is limited by the scarcity of commercially viable materials. This study evaluates high-pressure homogenization, a fully mechanical process, for producing micronized biopolymer particles as a sustainable feedstock for selective laser sintering. The biopolymer powder was characterized in terms of morphology and flowability, followed by processability validation on a selective laser sintering machine using both simple and more complex geometries. The resulting 3D printed components were assessed for dimensional accuracy and subjected to dynamic mechanical characterization. By offering an industrially scalable method for biopolymer powder production, high-pressure homogenization expands material options for selective laser sintering, advancing sustainable additive manufacturing.

## Introduction

Additive manufacturing (AM) of polymers has become essential for producing advanced plastic components in industries such as automotive, electronics, biomedical, and aerospace. Among AM techniques, material extrusion and vat photopolymerization are widely used due to their accessibility. However, material extrusion often results in coarse resolutions [1], while vat photopolymerization relies on thermoset resins that are difficult to recycle [2]. In contrast, Selective Laser Sintering (SLS) is a versatile and well-established AM method that enables the fabrication of complex, high-quality parts without support structures. Despite these advantages, one of the factors limiting the widespread adoption of SLS is the restricted commercial availability of polymer powders, which are predominantly synthetic materials such as polyamides [3].

The reliance on fossil-derived polymers raises environmental concerns, driving interest in biodegradable and bio-based alternatives that align with sustainability goals. Biopolymers have gained significant attention as eco-friendly materials in AM, with the polyhydroxyalkanoates (PHAs) standing out due to their tunable properties, cytocompatibility, and biodegradability under various environmental conditions [4]. Among PHAs, poly(3-hydroxybutyrate-*co*-3-hydroxyhexanoate) (PHBH) has emerged as a valuable candidate, offering a balance of mechanical strength and flexibility comparable to conventional plastics like polypropylene [5]. Derived from

Materials Research Proceedings 57 (2025) 154-163 https://doi.org/10.21741/9781644903735-18

bacterial fermentation of renewable feedstocks, PHBH might represent a sustainable alternative to petroleum-based polymers also for AM applications. Previous research on PHA powders for SLS has primarily focused on biomedical applications [6]. For instance, studies have demonstrated the feasibility of fabricating scaffolds for tissue engineering and assessing cell viability on SLS 3D printed structures [7,8]. However, a major limitation of existing approaches is the production method for biopolymer powders. Most studies have relied on solvent-induced phase separation, where a polymer solution is precipitated in an aqueous medium [9,10]. While this technique allows for controlled particle morphology and thermal stability, it suffers from low production yield and environmental drawbacks due to the extensive use of organic solvents. These challenges hinder the scalability and broader adoption of biopolymers in SLS.

To overcome these limitations, this study explores high-pressure homogenization (HPH) as a novel, solvent-free method for producing PHBH powder suitable for SLS. HPH is a purely mechanical process that enables efficient micronization of polymer particles, ensuring fine and uniform size distribution critical for successful SLS. The resulting powder was characterized in terms of morphology and flowability, two critical factors influencing powder bed homogeneity and processability in SLS. Additionally, 3D printed parts were examined for their dynamic mechanical properties and dimensional accuracy to assess the feasibility of PHBH powder obtained by HPH for SLS applications. By establishing a scalable, sustainable route for biopolymer powder production, this work expands the material options for SLS, with potential applicability to other biopolymers. Ultimately, this research contributes to bridging the gap between biopolymer development and practical implementation in AM, advancing the transition toward more sustainable manufacturing practices.

## Materials and Methods

### *Materials and equipment*

Poly(3-hydroxybutyrate-*co*-3-hydroxyhexanoate) (PHBH) pellets were purchased from MAIP Group (MAIP S.r.l., Settimo Torinese, Italy). Poly(vinyl alcohol) (PVA) 8-88 and silica oxide were obtained from Merck (Merck KGaA, Darmstadt, Germany). Glycerol EP 99% was supplied by ACEF (ACEF SpA, Fiorenzuola d'Arda, Italy). All materials were used as received, without further purification. For preliminary cryo-grinding, an A10 basic mill (IKA, Staufen, Germany) was used. HPH was then performed using a Panther NS3006L homogenizer (GEA Mechanical Equipment, Parma, Italy), equipped with a single-stage system, a pump for abrasive and viscous products, and a heat exchanger.

### *PHBH powder preparation*

The production process of PHBH powder consists of four main steps: cryo-grinding, suspension preparation, high-pressure homogenization, and final washing and drying. PHBH pellets were first cryo-ground using liquid nitrogen and sieved through a 1 mm mesh. The resulting powder was then dispersed at 1 wt.% in a medium composed of 50 wt.% glycerol and 50 wt.% aqueous PVA solution (5 wt.%). The suspension underwent high shear mixing at 3000 rpm before being processed via HPH, which included two initial passes at 300 bar, followed by 18 passes at 1000 bar. Sample coding was designated as NH for non-homogenized PHBH, while PHBH_H refers to the homogenized powders. After homogenization, the powder was filtered, washed with distilled water, and oven-dried at 50 °C overnight before being sieved through a 100 μm mesh. To improve flowability in SLS, the PHBH_H powder was blended with 0.25 wt.% silica oxide for 30 min, a method previously reported to enhance the processability of laboratory-produced polymer powders [11].

### *PHBH powder characterization*

The morphology of the PHBH powder was examined using a Phenom™ XL G2 Desktop scanning electron microscope (SEM) (Thermo Fisher Scientific, Waltham, MA, USA) operated at an

Materials Research Proceedings 57 (2025) 154-163 https://doi.org/10.21741/9781644903735-18

accelerating voltage of 20 kV. Prior to imaging, the powder was sputter-coated with gold for 180 s at a pressure of $10^{-3}$ mbar and a current of 10 mA (Complete Sputter Coating System, West Chester, PA, USA).

Particle size distribution (PSD) was analyzed using a Mastersizer 3000 laser granulometer (Malvern Panalytical, Malvern, UK), which utilizes laser diffraction to measure particle sizes in water-suspended samples. Data processing was performed using the Fraunhofer model, and the span was calculated based on particle size percentiles $D_{10}$, $D_{50}$, and $D_{90}$, representing the sizes below which 10%, 50%, and 90% of the total particle volume falls, respectively, following Eq. 1:

$$Span = \frac{D_{90} - D_{10}}{D_{50}} \tag{1}$$

Flowability was assessed by determining the compressibility index (C) and the Hausner ratio (HR). The parameters C and HR were measured using a simplified version of the ASTM D7481 standard with a 25 mL graduated cylinder, following Equations (2), (3), and (4), where $\rho_{bulk}$ and $\rho_{tap}$ denote the apparent and tapped densities of the PHBH powder, respectively.

$$C = \frac{\rho_{tap} - \rho_{bulk}}{\rho_{tap}} \times 100 \tag{2}$$

$$HR = \frac{\rho_{tap}}{\rho_{bulk}} \tag{3}$$

*Selective Laser Sintering*

Two different geometries were 3D printed using the same PHBH powder. First, bar-shaped samples (35 mm×10 mm×1 mm) were fabricated for thermomechanical analysis. Next, a small boat model was used as a reference part to evaluate the dimensional accuracy of SLS with PHBH powder feedstock. The boat has overall dimensions of 40 mm x 16 mm x 5.5 mm and features classical geometric elements that facilitate dimensional inspection. Figure 1 presents the CAD of the model boat.

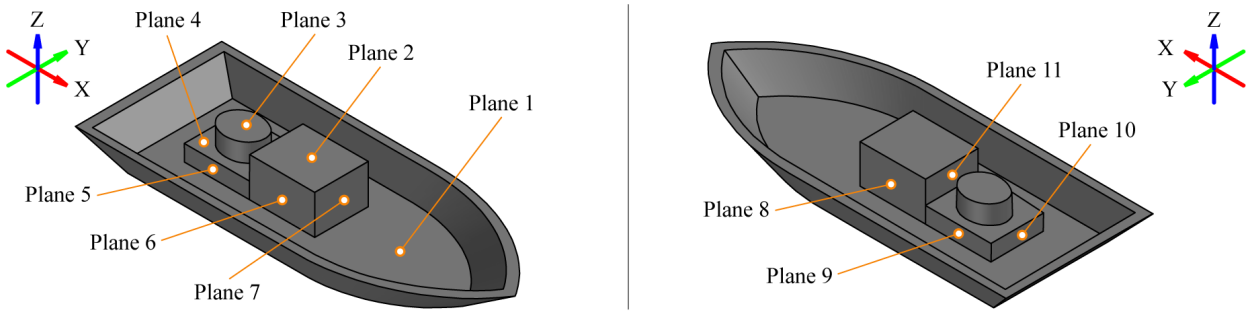


*Figure 1: Isometric view of the reference model with indication of the planes used for dimensional inspection*

Above the flat deck, two adjacent square blocks of different heights are positioned. These blocks own a base measuring 5.82 mm x 7.12 mm. The higher block has a height of 4.25 mm, while the smaller one is 1.75 mm high. Additionally, an elliptical block, standing 2 mm high, is placed on top of the smaller square block. The Cartesian reference frame is centered in the middle of the boat, with the Z-axis origin at the base of the hull, the positive Y-axis pointing port, and the

Materials Research Proceedings 57 (2025) 154-163 https://doi.org/10.21741/9781644903735-18

positive X-axis aligned with the bow. The following planes are considered to measure the heights and sizes of the different geometric features:

- Plane 1: Deck level at Z = 1.25 mm
- Plane 2: Top face of the larger square block at Z = 5.50 mm
- Plane 3: Top face of the elliptical block at Z = 5.00 mm
- Plane 4: Top face of the smaller square block at Z = 3.00 mm
- Plane 5: Right face (starboard) of the smaller square block at Y = −2.91 mm
- Plane 6: Right face (starboard) of the larger square block at Y = −2.91 mm
- Plane 7: Front face (bow) of the larger square block at X = 1.00 mm
- Plane 8: Left face (port) of the larger square block at Y = 2.91 mm
- Plane 9: Left face (port) of the smaller square block at Y = 2.91 mm
- Plane 10: Back face (stern) of the smaller square block at X = −13.24 mm
- Plane 11: Back face (stern) of the larger square block at X = −6.12 mm

All components were fabricated using a SnowWhite2 SLS machine (Sharebot S.r.l., Nibionno, Italy) equipped with a $CO_2$ laser operating at a wavelength of 10.6 μm. The biopolymer powder was evenly distributed in an air environment using a blade recoater. After reaching the target build chamber temperature, a 300 s waiting period was applied to ensure uniform heating of the powder bed. The key processing parameters are summarized in Table 1.

*Table 1: Selective laser sintering process parameters*

| **Process parameters** | |
|---|---|
| Laser power [W] | 3.5 |
| Scan speed [mm/s] | 2400 |
| Border scan speed [mm/s] | 3300 |
| Layer height [μm] | 100 |
| Environmental temperature [°C] | 90 |
| Number of warming layers | 50-150 |

*3D printed components characterization*

Dynamic mechanical analysis (DMA) was performed using an MCR 702e Multidrive Device (Anton Paar, Graz, Austria), applying a uniaxial sinusoidal stress with an amplitude of 1 N and a frequency of 1 Hz. A micro-CT scanner (X-CT) (Phoenix v|tome|x S240, GE Baker Hughes-Waygate Technologies, Wunstorf, Germany) was used to examine the 3D printed specimens, with the scanning parameters shown in Table 2. X-ray images were reconstructed into 3D models using datos|reconstruction software, and visualization and analysis were performed with VG Studio Max (version 3.4, Volume Graphics, Heidelberg, Germany). For dimensional analysis, surface determination was first carried out using the Advanced (classic) approach. This process involved contour identification from the histogram with an automatic material definition at an isovalue threshold of 50%.

*Table 2: X-CT scanning parameters*

| **Scanning parameters** | |
|---|---|
| Voxel size [μm] | 49.2 |
| Voltage [kV] | 210 |
| Current [μA] | 130 |
| Timing [ms] | 100 |
| Number of images | 1500 |

Materials Research Proceedings 57 (2025) 154-163 https://doi.org/10.21741/9781644903735-18

The Atos Compact Scan structured-light 3D scanner (Carl Zeiss AG, Oberkochen, Germany) was used for the scanning process. It is certified under the VDI/VDE 2637 standard for metrological performance. This device features two lateral CCD cameras for stereoscopic imaging and triangulation, along with a central projector for structured light projection. It has a 2-megapixel resolution, allowing it to capture around 2 million points per scan with 0.075 mm spacing and an accuracy of 0.02 mm. Belonging to safety class 2 (eye-safe), the scanner operates independently of ambient lighting. It utilizes a blue LED light source, which enhances stability by reducing performance fluctuations caused by heat buildup or changes in lighting conditions.

**Results and Discussions**

SEM analysis (Figure 2a, 2b) highlights the impact of homogenization on PHBH powders, showing a reduction in particle size due to compression, cavitation, shear forces, and impact over the homogenizing ring [12]. The powders exhibit an irregular morphology, likely due to plastic deformation at elevated processing temperatures (up to 70 °C) and high pressures.

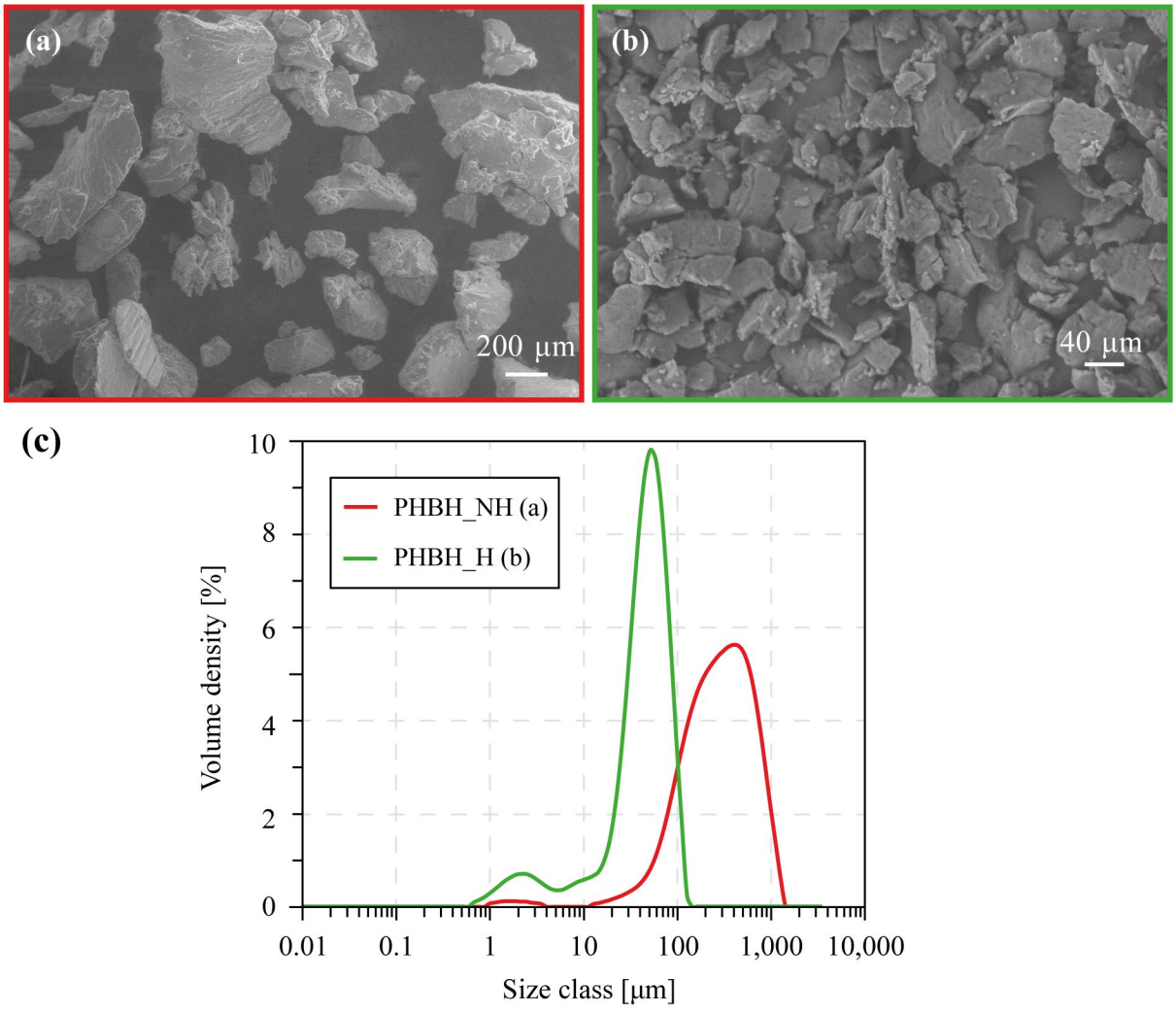


*Figure 2: Morphology analysis. SEM micrographs: PHBH_NH (a) and PHBH_H (b). Particle size granulometric curves: PHBH_NH (c) and PHBH_H (d)*

Granulometric analysis (Figure 2c) confirms size distributions of $D_{10}$, $D_{50}$, and $D_{90}$ at 105 µm, 313 µm, and 727 µm for PHBH_NH, and 11 µm, 49 µm, and 88 µm for PHBH_H. Both samples display a single-peaked distribution, with homogenization narrowing the peak and reducing span values from 2 to 1.6, indicating improved powder spreading [13].

Powder packing and flowability, crucial for SLS processing, were assessed via Hall flow and tap density tests, yielding a C value of 25.3%±0.1% and HR of 1.34±0.01. According to Carr's classification, PHBH_H exhibits "passable flowability" [14]. Morphological analysis supports this suboptimal flowability; however, past studies have shown that polymer-based composites with irregular morphologies can still be successfully processed via SLS [15,16]. Therefore, despite non-ideal flow properties, this preliminary characterization suggests PHBH powder from HPH is suitable for SLS applications.

The viscoelastic properties of 3D printed specimen were analyzed via DMA to assess their thermomechanical behavior. Figure 3 shows the extensional storage modulus and tan delta as functions of temperature. The glass transition temperature, determined from the tan delta peak, is 6 °C. The extensional storage modulus in the rigid plateau region is approximately 2.23 GPa, highlighting the potential of PHBH_H powder for SLS processing and its suitability for semi-structural applications, such as in the biomedical field [17].

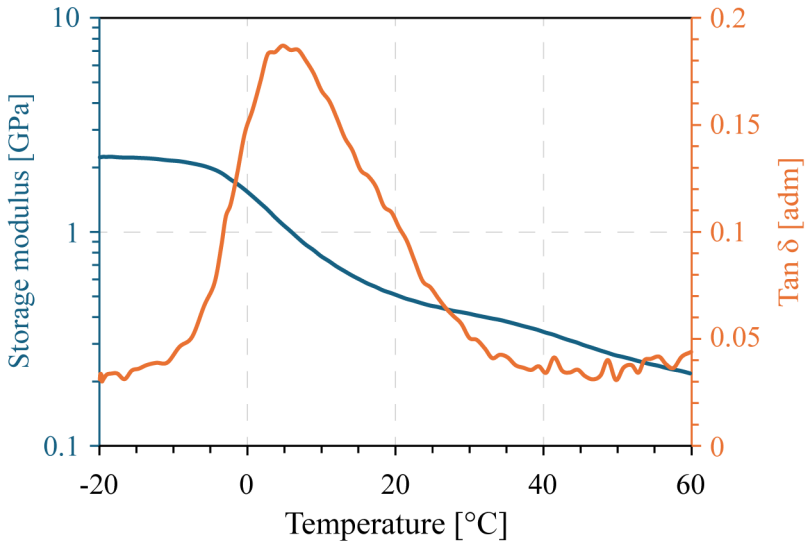


*Figure 3: DMA curves of 3D printed specimen of PHBH_H obtained by SLS*

To assess the 3D printability of PHBH_H powder using SLS, one replica of the boat model (Figure 1) was fabricated. Figure 4 shows the 3D printed replica (Fig. 4a) with a zoom-in of a central detail from the top view (Fig. 4b).

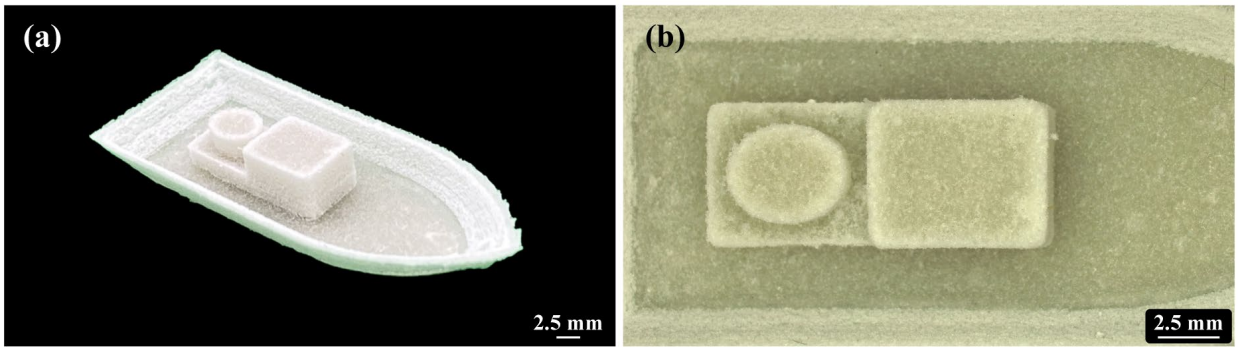


*Figure 4: 3D printed boat using PHBH_H powder: (a) SLS replica; (b) optical microscope image of a detail of the SLS replica*

The dimensional accuracy of the SLS replica was evaluated using GOM Inspect software by comparison of the actual scan data to the nominal CAD model. Figure 5 presents the colored map of nominal-to-actual deviations. Structured light optical scanning showed an average deviation of

Materials Research Proceedings 57 (2025) 154-163 https://doi.org/10.21741/9781644903735-18

0.28±0.28 mm (Fig. 5a), while X-CT scan measurements yielded a mean deviation of 0.11±0.28 mm (Fig. 5b). These results indicate good reproducibility of complex small geometries, though the deviation map highlights areas for optimization.

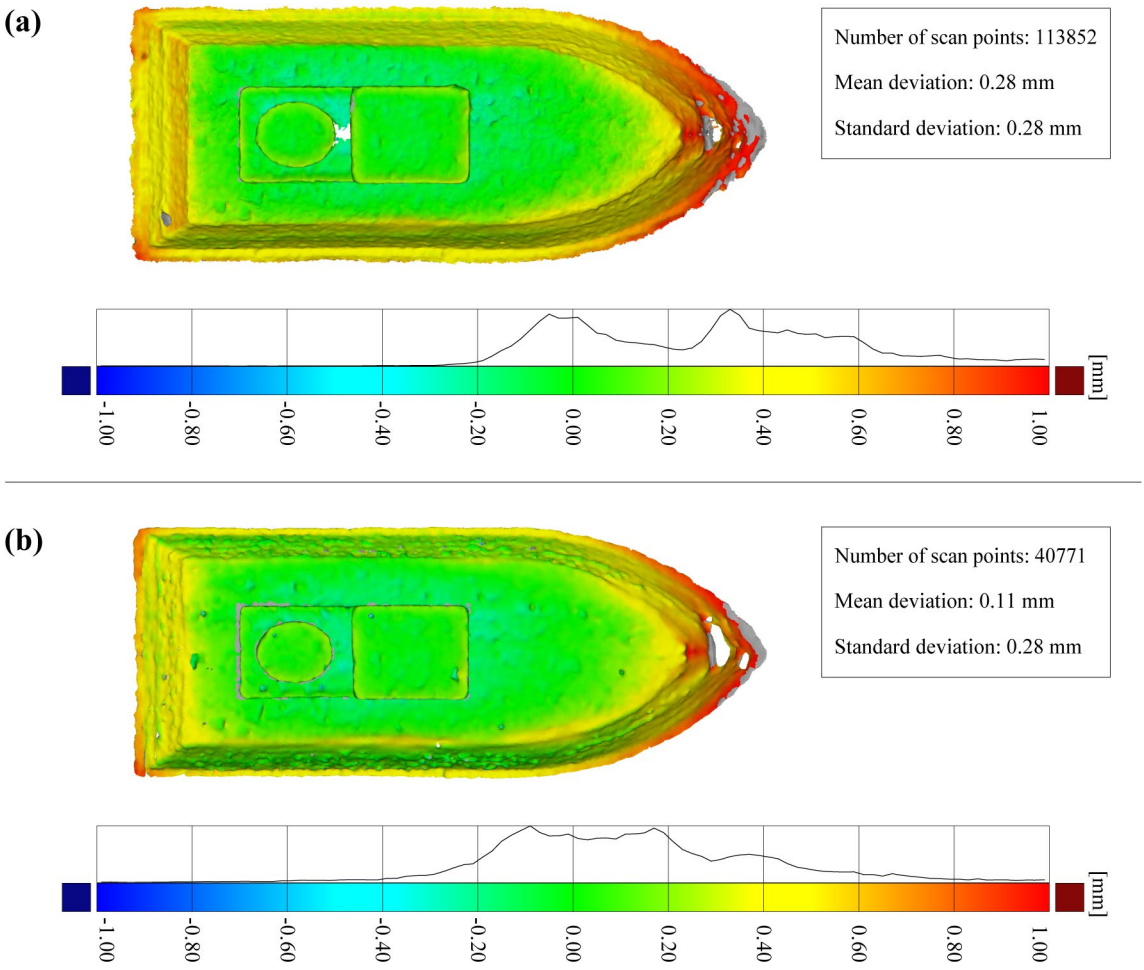


*Figure 5: Deviation analysis for the SLS replica from optical scan data (a) and X-CT data (b).*

As a bio-based polymer, PHBH undergoes thermal shrinkage upon cooling, contributing to negative dimensional deviations. Moreover, the spatial positioning of parts in the build chamber also affects heat dissipation and powder fusion, leading to anisotropic shrinkage. The highest deviations were observed at the bow and in tilted lateral zones, likely due to the difficulty of forming inclined thin walls, which are prone to material instability and distortions [18].

Table 3 summarizes key dimensional evaluations, referencing the planes in Figure 1, which play a crucial role in assessing dimensional accuracy. A comparison between X-CT and optical scanning reveals measurement discrepancies. While both methods provided consistent data for some features, such as the Z-height at Plane 1, larger discrepancies appeared in others, such as Plane 3, where X-CT recorded 5.26 mm and optical scanning measured 5.20 mm, deviating from the nominal 5.00 mm. Similarly, along the Y-axis, deviations were found between Plane 6 and Plane 8, with X-CT measuring 5.65 mm and optical scanning 6.02 mm. These differences may result from resolution limitations, surface reflectivity, or occlusions during optical scanning, as previously reported in studies evaluating the accuracy of 3D scanning techniques for polymer-based materials [19].

*Table 3: Dimensional analysis of the boat model with optical scanner and X-CT*

| Dimensional evaluations (all values are in mm) | Nominal value | Actual values | |
|---|---|---|---|
| | | X-CT | Scanner |
| Z-height Plane 1 | 1.25 | 1.06 | 1.06 |
| Z-height Plane 2 | 5.50 | 5.50 | 5.48 |
| Z-height Plane 3 | 5.00 | 5.26 | 5.20 |
| Z-height Plane 4 | 3.00 | 2.69 | 2.69 |
| Distance Plane 5 - Plane 9 along Y-axis | 5.82 | 5.77 | 6.01 |
| Distance Plane 6 - Plane 8 along Y-axis | 5.82 | 5.65 | 6.02 |
| Distance Plane 7 - Plane 10 along X-axis | 14.24 | 14.03 | 14.31 |
| Distance Plane 10 - Plane 11 along X-axis | 7.08 | 7.15 | 7.37 |

To improve dimensional accuracy, further optimization is needed. Optimization strategies may include refining processing parameters like laser power, hatch spacing, and scan strategies to enhance feature fidelity. Thermal compensation models could minimize shrinkage effects, while post-processing techniques such as surface treatments or annealing may help reduce warping. These findings suggest PHBH has strong potential for sustainable SLS applications, warranting further research to enhance precision and reproducibility. Understanding the interplay between processing conditions and material behavior will be key to advancing PHBH for industrial additive manufacturing.

## Conclusions

This study demonstrated the feasibility of HPH as a scalable and sustainable method for producing biopolymer powders for SLS, providing an efficient alternative to previously explored techniques. The HPH process successfully micronized PHBH, achieving a median particle size of 49 μm. Despite their irregular morphology, flowability tests confirmed the powders' suitability for SLS processing. The powders enabled the fabrication of both simple and complex geometries. For dynamic mechanical property testing, the 3D printed samples exhibited a maximum storage modulus of 2.23 GPa. Additionally, a more intricate geometry, such as the boat model, was successfully produced with good dimensional accuracy. Optical scanning analysis of the 3D printed part revealed an average deviation of 0.28 mm from the nominal CAD surface, suggesting the reliability of the powder for SLS applications. This work contributes to bridging the gap between laboratory-scale powder development and industrial production. Future research should focus on optimizing powder morphology and flowability, refining SLS process parameters, and enhancing HPH productivity to further improve its competitiveness. By utilizing a purely mechanical approach, this study underscores the potential of HPH produced biopolymer powders for sustainable AM, paving the way for greener applications.

## References

[1] G. D. Goh, Y. L. Yap, H. K. J. Tan, S. L. Sing, G. L. Goh, W. Y. Yeong, Process–Structure–Properties in Polymer Additive Manufacturing via Material Extrusion: A Review, Crit Rev Solid State 45 (2020) 113-133. https://doi.org/10.1080/10408436.2018.1549977

[2] A. Davoudinejad, Vat photopolymerization methods in additive manufacturing, in: J. Pou, A. Riveiro, J. P. Davim (Eds.), Additive Manufacturing, Elsevier, 2021, pp. 159–181. https://doi.org/10.1016/B978-0-12-818411-0.00007-0

[3] P. C. Gomes, O. G. Piñeiro, A. C. Alves, O. S. Carneiro, On the Reuse of SLS Polyamide 12 Powder, Materials 15 (2022) 5486. https://doi.org/10.3390/ma15165486

[4] S. Bano, A. A. Aslam, A. Khan, A. Shabbir, F. Qayyum, N. Wahab, A. Jabar, I. Ul Islam, S. L. Ng, A mini-review on polyhydroxyalkanoates: Synthesis, extraction, characterization, and applications, Process Biochem 146 (2024) 250-261. https://doi.org/10.1016/j.procbio.2024.07.033

[5] K. Eraslan, C. Aversa, M. Nofar, M. Barletta, A. Gisario, R. Salehiyan, Y. A. Goksu, Poly(3-hydroxybutyrate-co-3-hydroxyhexanoate) (PHBH): Synthesis, properties, and applications - A review, Eur Polym J 167 (2022) 111044. https://doi.org/10.1016/j.eurpolymj.2022.111044

[6] V. Volpini, A. Giubilini, L. Corsi, A. Nobili, F. Bondioli, Characterization of biocompatible scaffolds manufactured by fused filament fabrication of poly(3-hydroxybutyrate-co-3-hydroxyhexanoate), R. Soc. Open Sci. 9 (2022) 211485. https://doi.org/10.1098/rsos.211485

[7] B. Duan, M. Wang, W. Y. Zhou, W. L. Cheung, Z. Y. Li, W. W. Lu, Three-dimensional nanocomposite scaffolds fabricated via selective laser sintering for bone tissue engineering, Acta Biomater 6 (2010) 4495-4505. https://doi.org/10.1016/j.actbio.2010.06.024

[8] B. Duan, W. L. Cheung, M. Wang, Optimized fabrication of Ca–P/PHBV nanocomposite scaffolds via selective laser sintering for bone tissue engineering, Biofabrication 3 (2011) 015001. https://doi.org/10.1088/1758-5082/3/1/015001

[9] B. Duan, M. Wang, Customized Ca–P/PHBV nanocomposite scaffolds for bone tissue engineering: design, fabrication, surface modification and sustained release of growth factor, J R Soc Interface 7 (2010) S615. https://doi.org/10.1098/rsif.2010.0127.focus

[10] A. Giubilini, G. Colucci, G. De Trane, F. Lupone, C. Badini, P. Minetola, F. Bondioli, M. Messori, Novel 3D printable bio-based and biodegradable poly(3-hydroxybutyrate-co-3-hydroxyhexanoate) microspheres for selective laser sintering applications, Mater Today Sustain 22 (2023) 100379. https://doi.org/10.1016/j.mtsust.2023.100379

[11] K. T. Kunnath, S. Tripathi, S. S. Kim, L. Chen, K. Zheng, R. N. Davé, Selection of Silica Type and Amount for Flowability Enhancements via Dry Coating: Contact Mechanics Based Predictive Approach, Pharm Res 40 (2023) 2917-2933. https://doi.org/10.1007/s11095-023-03561-6

[12] R. Levy, Z. Okun, A. Shpigelman, High-Pressure Homogenization: Principles and Applications Beyond Microbial Inactivation, Food Eng Rev 13 (2021) 490-508. https://doi.org/10.1007/s12393-020-09239-8

[13] M. Schmid, A. Amado, K. Wegener, Polymer powders for selective laser sintering (SLS), AIP Conf Proc 1664 (2015) 160009. https://doi.org/10.1063/1.4918516

[14] A. T. Sutton, C. S. Kriewall, M. C. Leu, J. W. Newkirk, Powder characterisation techniques and effects of powder characteristics on part properties in powder-bed fusion processes, Virtual Phys Prototyp 12 (2017) 3-29. https://doi.org/10.1080/17452759.2016.1250605

[15] F. Lupone, E. Padovano, V. G. Lambertini, R. Sampieri, F. Casamento, S. Zecchi, C. Badini, Selective Laser Sintering versus Multi Jet Fusion: A Comprehensive Comparison Study Based on the Properties of Glass Beads-Reinforced Polyamide 12, Adv Eng Mater 26 (2024) 2301345. https://doi.org/10.1002/adem.202301345

[16] R. Ajdary, N. Kretzschmar, H. Baniasadi, J. Trifol, J. V Seppälä, J. Partanen, O. J. Rojas, Selective Laser Sintering of Lignin-Based Composites, ACS Sustain Chem Eng 9 (2021) 2727-2735. https://doi.org/10.1021/acssuschemeng.0c07996

[17] J. Ivorra-Martinez, L. Quiles-Carrillo, T. Boronat, S. Torres-Giner, J. A. Covas, Assessment of the Mechanical and Thermal Properties of Injection-Molded Poly(3-hydroxybutyrate-co-3-

hydroxyhexanoate)/Hydroxyapatite Nanoparticles Parts for Use in Bone Tissue Engineering, Polymers 12 (2020) 1389. https://doi.org/10.3390/polym12061389

[18] H. Z. Shen, N. A. Muhayudin, K. S. Basaruddin, S. F. K. M. Khan, L. Tajul, T. D. Hoang, Benchmarking artifact of selective laser sintering (SLS) components fabricated with exible and rigid polymers, Eng. Res. Express 7 (2025) 015409. https://doi.org/10.1088/2631-8695/ada48c

[19] M. Kritikos, J. Urminsky, I. Buransky, Comparison of Optical Scanner and Computed Tomography Scan Accuracy, Lect Notes Mech. Eng (2022) 521-530. https://doi.org/10.1007/978-3-030-90421-0_44